IEEE Access
Multidisciplinary | Rapid Review | Open Access Journal

Received February 21, 2022, accepted March 14, 2022, date of publication March 21, 2022, date of current version April 1, 2022.

Digital Object Identifier 10.1109/ACCESS.2022.3161056

Multivariable Bi-Objective Optimal Modification Adaptive Control for Turbofan Engine With Matched Uncertainty and Slow Actuator Dynamics

MEIYIN ZHU[1,2], XI WANG[2,3], SHUBO YANG[2,3], KEQIANG MIAO[2,3], XITONG PEI[2,3], JIASHUAI LIU[2,3], AND LOUYUE ZHANG[2,3]

[1]Beihang Hangzhou Innovation Institute Yuhang, Hangzhou 310023, China
[2]School of Energy and Power Engineering, Beihang University, Beijing 100191, China
[3]Collaborative Innovation Center for Advanced Aero-Engine, Beijing 100191, China

Corresponding author: Shubo Yang (xjysb@qq.com)

This work was supported in part by the National Science and Technology Major Project, China, under Grant 2017-V-0015-0067; in part by the China Scholarship Council under Grant 201906020036; in part by AECC Sichuan Gas Turbine Establishment Stable Support Project under Grant GJCZ-0011-19; and in part by the Academic Excellence Foundation of BUAA for Ph.D. degree Students under Grant BY1604166.

ABSTRACT To address the multivariable control problem of turbofan engines with matched uncertainty and slow actuator dynamics (SAD), a bi-objective optimal modification adaptive control scheme is proposed. A singular perturbation approach is introduced to transform the plant and actuator dynamics into a reduced-order system with slow time coordinate. Based on this reduced-order system, the bi-objective optimal modification adaptive law (BOMAL) is deduced. Meanwhile, the stability of BOMAL is analyzed based on Lyapunov approach. The simulation results demonstrate that the proposed adaptive control method can effectively handle the control problem of turbofan engines with SAD. The superiority of the proposed bi-objective optimal modification adaptive controller is benchmarked with an LMI optimization gain scheduled controller and a μ synthesis controller.

INDEX TERMS Turbofan engine, model reference adaptive control, bi-objective, optimal control modification, uncertainty, slow actuator dynamics.

I. INTRODUCTION

Turbofan engines are one of the most important propulsion systems in aviation industry. Because of the advantage of lower fuel consumption and higher reliability comparing with those of other jet engines, turbofan engines are widely used for military and commercial aircrafts [1]. The control system is required to regulate the engine to provide good thrust control performance while keeping all the key engine outputs within safety limits during lifetime of the engine [2]. Although the current control system of turbofan engines employs full authority digital electronics system, its actuator usually constructed by hydraulic mechanical structure. The dynamic characteristics of the actuators are relatively slow compared with the controlled object. Due to aging, performance degradation of the components, and motion wear, the dynamic performance of the actuators may further deteriorate. Slow actuator dynamics (SAD), especially when the actuators suffer from performance degradation, have negative influence on dynamic performance of the closed-loop system. Therefore, considering SAD in the control design is significant, it can also enhance robustness of the designed controller.

However, in most studies, the actuator dynamics are not considered or assumed as fast dynamics in the control design. Pan *et al.* [3] studied robust decentralized control for aircraft engines without considering actuator dynamics. Du *et al.* [4] investigated the design of scheduled adaptive model predictive control for turbofan engines, however, they did not consider actuator dynamics. Chen *et al.* [5] considered a fast actuator dynamics in their study on decoupling control design for turboprop engines. Miao *et al.* [6] studied the transient control problem of turbofan engines with fast actuator dynamics by using Linear Matrix Inequality (LMI)

The associate editor coordinating the review of this manuscript and approving it for publication was Engang Tian.

optimization. Liu *et al.* [7] assumed a fast actuator dynamics in their study on multivariable adaptive control for turbofan engine. Generally, due to the existence of SAD and unmodeled uncertainties, it is challenging to consider SAD and uncertainties in the adaptive controller design to ensure robustness. Therefore, a critical issue about finding a robust adaptive controller for turbofan engines with SAD and uncertainties is yet to be solved, that is, does there exist a model reference adaptive controller to realize robust stability? However, there have been no relevant theoretical results available, which motivates our study. To consider SAD and uncertainties in the control design of turbofan engines, we propose a new Model Reference Adaptive Control (MRAC) scheme with bi-objective optimal modification based on the Singularly Perturbed System (SPS). The motivation for introducing Singular Perturbation Approach (SPA) is to transform the plant and SAD into a reduced-order system to obtain the Bi-objective Optimal Modification Adaptive Law (BOMAL). The motivation for choosing adaptive control is to take the advantage of processing uncertainty and to utilize the flexibility of control structure.

Recently, with the study and development of adaptive control theory, adaptive control has been widely applied in many important engineering areas, such as aircraft engine [7]–[9], industrial [10]–[12], UAVs [13], altitude ground test facilities [14], etc. In addition, many MRAC approaches have been proposed to provide robustness for system with uncertainty [14], [15]. To enhance the robustness of the conventional MRAC, several robust modification approaches such as adaptive loop recovery modification [16], dead-zone modification [17], and Optimal Control Modification (OCM) [18] have been considered. The OCM is formulated from the optimal control theory as an adaptive optimal control method. Until now, the optimal control theory has been successfully applied in many engineering areas, such as [18]–[20] and so on. The optimal control framework has been combined with adaptive or fuzzy control to address robust problem, such as unknown dynamics [19], time delay [20] and so on. The OCM technique is an important application of optimal control in adaptive control, which was first proposed by Nguyen and rigorously validated through F/A-18A airplane flight tests [21]. During the last few years, many extensions of the OCM method has been developed. The OCM adaptive control is used to improve tracking performance of systems with SAD [22]. Nguyen used the OCM method to improve control effectiveness of systems with both matched and control input uncertainty [23]. The OCM method is used to address robust control of flight environment simulation system with disturbance and large heat transfer uncertainty [14]. For system with unknown control input matrix Λ, the OCM method cannot obtain the adaptive law. To compensate the limitation of the OCM, the bi-objective OCM method has been developed by adding one extra cost function arisen from a predictor model to the OCM method [24], [25].

The main contributions are listed as follows:(i) Inclusion of SAD of a turbofan engine in the control design for the first time.(ii) Application of the SPA to transform the plant and actuator dynamics into a reduced-order system. (iii) Providing a solution to address robust control of turbofan engines with SAD. This paper is organized as follows. The transformation of the plant and actuator dynamics into a reduced-order system with slow time coordinate is presented Section 2. Section 3 deduces the BOMAL. The simulation study and some conclusions are presented in Section 4 and 5 respectively.

II. REDUCED-ORDER SYSTEM WITH SLOW TIME

Consider a linear plant with matched uncertainty

$$\dot{x} = Ax + B\left(u + \Omega^{*T} x\right) \tag{1}$$

where $x(t) \in \mathbb{R}^n$ is a state vector, $u(t) \in \mathbb{R}^m$ is a control input vector, $A \in \mathbb{R}^{n\times n}$ is a known and constant Hurwitz matrix, $B \in \mathbb{R}^{n\times m}$ is a known constant matrix, the pair (A, B) is controllable, and $\Omega^* \in \mathbb{R}^{n\times m}$ is a unknown constant matrix.

The controller $u(t)$ with SAD is specified as

$$\dot{u} = \varepsilon M (u - v) \tag{2}$$

where $v(t) \in \mathbb{R}^m$ is the input of actuators, ε is a positive constant, and $M \in \mathbb{R}^{n\times m}$ is a known and constant Hurwitz matrix.

The objective is to design a controller $u(t)$ that enables the plant to follow a reference model specified as

$$\dot{x}_m = A_m x_m + B_m r \tag{3}$$

where $x_m(t) \in \mathbb{R}^n$ is a reference state vector, $r(t) \in \mathbb{R}^q$ is a bounded reference command vector, $A_m \in \mathbb{R}^{n\times n}$ is known and Hurwitz, and $B_m \in \mathbb{R}^{n\times q}$is a known matrix associated with a piecewise continuous.

If the actuators dynamics are sufficiently fast relative to the dynamics of the reference model, namely, $\varepsilon \|M\| \geq \|A_m\|$, then the influence of actuator dynamics is negligible and the adaptive law can be designed by using the conventional adaptive method. However, in our case, the actuator dynamics is slow with $\varepsilon \ll 1$ and $\varepsilon \|M\| \ll \|A_m\|$, which means $u(t)$ has 'slow' dynamics and $x(t)$ has 'fast' dynamics. To decouple the slow state $u(t)$ and fast state $x(t)$, a timescale separation is performed through applying the SPA. Therefore, a slow time transformation is considered as

$$\tau = \varepsilon t \tag{4}$$

where τ is a slow time variable.

Remark 1: It is noted that the conventional method to address actuator dynamics by augmenting with the plant is not suitable for adaptive control. After augmenting, the state of the augmented system increased which will mismatch with the reference model. Therefore, we introduce the singular perturbation approach to transform the plant and actuator dynamics into a reduced-order system with slow time coordinate to address the problem.

Thus, we transform the plant (1) and actuator (2) into a SPS as

$$\begin{cases} \varepsilon \dfrac{dx}{d\tau} = Ax + B\left(u + \Omega^{*T} x\right) \\ \dfrac{du}{d\tau} = M\left(u - v\right) \end{cases} \tag{5}$$

By setting $\varepsilon = 0$, the solution of the SPS can be approximated with the solution of a 'reduced-order' system by using the Tikhonov's theorem [26]. Thus, $x(u, \varepsilon)$ is on a fast manifold. The fast dynamics results in $x(u, \varepsilon)$ tending to its asymptotic solution as $\varepsilon \to 0$. Therefore, the reduced-order system is obtained as

$$\begin{cases} \varepsilon \dfrac{dx_o}{d\tau} = Ax_o + B\left(u_o + \Omega^{*T} x_o\right) = 0 \\ \dfrac{du_o}{d\tau} = M\left(u_o - v\right) \end{cases} \tag{6}$$

where $x_o(\tau)$ and $u_o(\tau)$ are the 'outer' solution of the SPS.

The 'outer' and 'inner' or 'boundary layer' solutions origin from the boundary layer theory [27]. The 'inner' or 'boundary layer' solution for this system can be obtained from

$$\begin{cases} \dot{x}_{in} = Ax_{in} + B\left(u_{in} + \Omega^{*T} x_{in}\right) \\ \dot{u}_{in} = \varepsilon M\left(u_{in} - v\right) = 0 \end{cases} \tag{7}$$

The solution of $x(t)$ is then expressed as

$$x(t) = x_o(t) + x_{in}(t) - x_{MAE}(t) \tag{8}$$

where $x_{MAE}(t)$ is a correction term.

Remark 2: The 'outer' solution is actually the asymptotic solution of the original system as $t \to \infty$.

From the reduced-order system (6), we obtain the solution of $x_o(\tau)$ as

$$x_o(\tau) = -\left(A + B\Omega^{*T}\right)^{-1} B u_o(\tau) \tag{9}$$

Differentiating the above equation with respect to τ and then substituting the actuator model in (6) into the result yield

$$\frac{dx_o}{d\tau} = -\left(A + B\Omega^{*T}\right)^{-1} BM\left(u_o - v\right) \tag{10}$$

From (6), we have

$$u_o = -\tilde{B}^{-1} A x_o - \Omega^{*T} x_o \tag{11}$$

where $\tilde{B}^{-1} = \left(B^T B\right)^{-1} B^T$ is the right pseudo-inverse of B.

Therefore, the reduced-order system constrained by SAD is obtained as

$$\frac{dx_o}{d\tau} = \left(A + B\Omega^{*T}\right)^{-1} BM\left(\tilde{B}^{-1} A x_o + \Omega^{*T} x_o + v\right) \tag{12}$$

Lemma 1 [28]: For matrices X, Y, and Z with appropriate dimension, the following equation satisfies

$$(X + YZ)^{-1} = X^{-1} - X^{-1} Y\left(I + ZX^{-1} Y\right)^{-1} ZX^{-1} \tag{13}$$

Using Lemma 1, we obtain

$$\left(A + B\Omega^{*T}\right)^{-1} = A^{-1} - A^{-1} B\left(I + \Omega^{*T} A^{-1} B\right)^{-1} \Omega^{*T} A^{-1} \tag{14}$$

Letting $\Psi^{*T} = A^{-1} B\left(I + \Omega^{*T} A^{-1} B\right)^{-1} \Omega^{*T} A^{-1}$ and substituting it into (12), we obtain

$$\begin{aligned} \frac{dx_o}{d\tau} = {} & A^{-1} BM\tilde{B}^{-1} A x_o + \big[- \Psi^{*T} BM\tilde{B}^{-1} A \\ & + \left(A^{-1} - \Psi^{*T}\right) BM\Omega^{*T} \big] x_o + \left(A^{-1} - \Psi^{*T}\right) BMv \end{aligned} \tag{15}$$

In our study, we just need to consider asymptotic solution of (5). Thus, the 'inner' solution can be neglected such that $x(t) = x_o(t)$. Then, the reduced-order system (15) can be expressed as

$$\frac{dx}{d\tau} = A_P x + B_P \Lambda\left(v + \Omega_P^{*T} x\right) \tag{16}$$

where $A_P = A^{-1} BM\tilde{B}^{-1} A$, $B_P = A^{-1} BM$, and $B_P \Lambda \Omega_P^{*T} = \left(A^{-1} - \Psi^{*T}\right) BM\Omega^{*T} - \Psi^{*T} BM\tilde{B}^{-1} A$.

Considering the influence of SAD, the time scale of the plant response cannot surpass that of the actuator. To avoid model mismatch, we revise the reference model in slow time to match the slow actuator constrained system as

$$\frac{dx_m}{d\tau} = \frac{1}{\varepsilon}\left(A_m x_m + B_m r\right) \tag{17}$$

III. BI-OBJECTIVE OPTIMAL MODIFICATION ADAPTIVE LAW

Firstly, a fixed gain controller is devised to stabilize the system (1) when without uncertainty and SAD

$$\bar{u} = K_x x + K_r r \tag{18}$$

where, K_x and K_r are obtained from the following ideal model matching condition

$$\begin{cases} A_m = A + BK_x \\ B_m = BK_r \end{cases} \tag{19}$$

Then, we choose the adaptive control structure for the input signal of actuator as

$$v = \bar{u} - u_{ad} = \bar{u} + \Delta K_x(\tau) x + \Delta K_r(\tau) r - \Omega_P^T(\tau) x \tag{20}$$

Assumption 1: [14] There exist two ideal control gain matrices ΔK_x^* and ΔK_r^* that satisfy the model matching conditions as

$$\begin{cases} \dfrac{1}{\varepsilon} A_m = A_P + B_P \Lambda\left(K_x + \Delta K_x^*\right) \\ \dfrac{1}{\varepsilon} B_m = B_P \Lambda\left(K_r + \Delta K_r^*\right) \end{cases} \tag{21}$$

Remark 3: The existence condition of the two ideal control gain matrices ΔK_x^* and ΔK_r^* is that Ω^* is full row rank. Because A_m, B_m, A_P, B_P, K_x, and K_r are known matrices, if the right pseudo-inverse of $B_P \Lambda$ is exist, according to the Eq. (21), we obtain

$$\begin{cases} \Delta K_x^* = \left(B_P \Lambda\right)^{-R}\left(\dfrac{1}{\varepsilon} A_m - A_P\right) - K_x \\ \Delta K_r^* = \dfrac{1}{\varepsilon}\left(B_P \Lambda\right)^{-R} B_m - K_r \end{cases}$$

where, $(B_P\Lambda)^{-R} = \left[(B_P\Lambda)^T (B_P\Lambda)\right]^{-1} (B_P\Lambda)^T$ is the right pseudo-inverse of $B_P\Lambda$. Therefore, the existence condition of the two ideal control gain matrices ΔK_x^* and ΔK_r^* is that is $B_P\Lambda$ full row rank. According to (15) and (16), we have

$$\begin{cases} B_P\Lambda = \left(A^{-1} - \Psi^{*T}\right) BM \\ \Psi^{*T} = A^{-1}B\left(I + \Omega^{*T}A^{-1}B\right)^{-1}\Omega^{*T}A^{-1} \end{cases}$$

Since A is full rank, B is full row rank, and M is full rank, if Ω^* is full row rank, $B_P\Lambda$ is full row rank.

We define $\Delta\tilde{K}_x(\tau) = \Delta K_x(\tau) - \Delta K_x^*$, $\Delta\tilde{K}_r(\tau) = \Delta K_r(\tau) - \Delta K_r^*$, and $\tilde{\Omega}_P^T(\tau) = \Omega_P^T(\tau) - \Omega_P^{*T}$ as estimation errors. By substituting (20) into (16), the closed-loop system in slow time is obtained as

$$\frac{dx}{d\tau} = \frac{1}{\varepsilon}A_m x + \frac{1}{\varepsilon}B_m r + B_P\Lambda(\Delta\tilde{K}_x(\tau)x + \Delta\tilde{K}_r(\tau)r - \tilde{\Omega}_P^T(\tau)x) \quad (22)$$

Thus, we obtain the tracking error equation in slow time as

$$\frac{de}{d\tau} = \frac{dx_m}{d\tau} - \frac{dx}{d\tau} = \frac{1}{\varepsilon}A_m e - B_P\Lambda(\Delta\tilde{K}_x(\tau)x + \Delta\tilde{K}_r(\tau)r - \tilde{\Omega}_P^T(\tau)x) \quad (23)$$

If Λ is a diagonal matrix with known sign, the adaptive controller in real time can be obtained by using the modified optimal adaptive method in [28] as

$$\dot{\Theta} = -\varepsilon\Gamma_\Theta\Phi(x, r)\left[e^T P sgn\Lambda - \varepsilon\gamma\Phi^T(x, r)\Theta B_P^T P A_m^{-1}\right]B_P \quad (24)$$

where $\Theta^T(t) = \left[\Omega_P^T(t) - \Delta K_x(t) - \Delta K_r(t)\right] \in R^{m\times n+q}$ and $\Phi(x, r) = \left[x^T r^T\right]^T \in R^{n+q}$, $\gamma > 0 \in \mathbb{R}$ is the modification parameter, $\Gamma_\Theta = \Gamma_\Theta^T \in R^{n+q\times n+q}$ is a positive-definite adaption rate matrix for $\Theta^T(t)$, and $P = P^T > 0 \in \mathbb{R}^{n\times n}$.

However, in our case, Λ is unknown. To estimate Λ, we introduce the following predictor model in slow time as

$$\frac{d\hat{x}}{d\tau} = \frac{1}{\varepsilon}A_m\hat{x} + \left(A_P - \frac{1}{\varepsilon}A_m\right)x + B_P\hat{\Lambda}\left(v + \Omega_P^T(\tau)x\right) \quad (25)$$

We define $\tilde{\Lambda}(\tau) = \hat{\Lambda}(\tau) - \Lambda$ and substitute into (23), the tracking error becomes

$$\frac{de}{d\tau} = \frac{1}{\varepsilon}A_m e - B_P\hat{\Lambda}(\Delta\tilde{K}_x(\tau)x + \Delta\tilde{K}_r(\tau)r - \tilde{\Omega}_P^T(\tau)x) + B_P\sigma \quad (26)$$

where $\sigma(\tau) = \tilde{\Lambda}(\Delta\tilde{K}_x(\tau)x + \Delta\tilde{K}_r(\tau)r - \tilde{\Omega}_P^T(\tau)x)$ is the residual estimation error of the system with $sup\,\|\sigma(\tau)\| \le \sigma_0$.

The predictor error in slow time is defined as $e_P(\tau) = \hat{x}(\tau) - x(\tau)$, then

$$\frac{de_P}{d\tau} = \frac{1}{\varepsilon}A_m e_P + B_P\tilde{\Lambda}\left(v + \Omega_P^T(\tau)x\right) + B_P\hat{\Lambda}\tilde{\Omega}_P^T(\tau)x + B_P\sigma_P \quad (27)$$

where $\sigma_P(\tau) = -\tilde{\Lambda}\tilde{\Omega}_P^T(\tau)x$ is the residual estimation error of the predictor model with $sup\,\|\sigma_P(\tau)\| \le \sigma_{P0}$.

To obtain the adaptive law with unknown Λ and ensure robustness of the adaptive controller, we introduce a BOMAL. The BOMAL is derived from the following two infinite-time horizon cost functions

$$\begin{cases} J_1 = \lim\limits_{\tau_f\to\infty}\dfrac{1}{2}\displaystyle\int_0^{\tau_f}(e - \Delta_1)^T Q(e - \Delta_1)\,d\tau \\ J_2 = \lim\limits_{\tau_f\to\infty}\dfrac{1}{2}\displaystyle\int_0^{\tau_f}(e_P - \Delta_2)^T W(e_P - \Delta_2)\,d\tau \end{cases} \quad (28)$$

where, $\Delta_1(\tau)$ and $\Delta_2(\tau)$ denote unknown lower bound of $e(\tau)$ and $e_P(\tau)$ respectively, and $Q = Q^T > 0 \in \mathbb{R}^{n\times n}$ and $W = W^T > 0 \in \mathbb{R}^{n\times n}$.

To minimize $e(\tau)$ and $e_P(\tau)$ bounded away from the origin, the cost functions J_1 and J_2 are considered into the following bi-objective cost function

$$J = J_1 + J_2 \quad (29)$$

Remark 4: The bi-objective cost function J combines both the objectives of minimization of the tracking error and the predictor error bounded away from the origin. Geometrically, it represents the sum of the weighted norm squares measured from the trajectories of e and e_P to the normal surface of a hyper-sphere as follows

$$B_\Delta = \left\{e, e_P \in \mathbb{R}^n : (e - \Delta_1)^T Q(e - \Delta_1) + (e_P - \Delta_2)^T W(e_P - \Delta_2) \le \Delta^2\right\}$$

Then, the Hamiltonian Function is defined by using the optimal control framework [28] as

$$\begin{aligned} &H\left(e, e_P, \Delta\tilde{K}_x, \Delta\tilde{K}_r, \tilde{\Omega}_P, \tilde{\Lambda}\right) \\ &= \frac{1}{2}(e - \Delta_1)^T Q(e - \Delta_1) + \frac{1}{2}(e_P - \Delta_2)^T W(e_P - \Delta_2) \\ &\quad + \eta^T\left[\frac{1}{\varepsilon}A_m e - B_P\hat{\Lambda}\left(\Delta\tilde{K}_x(\tau)x + \Delta\tilde{K}_r(\tau)r - \tilde{\Omega}_P^T(\tau)x\right)\right. \\ &\quad \left. + B_P\sigma\right] + \mu^T\left[\frac{1}{\varepsilon}A_m e_P + B_P\tilde{\Lambda}\left(v + \Omega_P^T(\tau)x\right)\right. \\ &\quad \left. + B_P\hat{\Lambda}\tilde{\Omega}_P^T(\tau)x + B_P\sigma_P\right] \end{aligned} \quad (30)$$

where $\eta(\tau) \in \mathbb{R}^n$ and $\mu(\tau) \in \mathbb{R}^n$ are adjoint vectors.

From the necessary condition of optimality, we obtain the adjoint equations as

$$\begin{cases} \dfrac{d\eta}{d\tau} = -\nabla H_e^T = -Q(e - \Delta_1) - \dfrac{1}{\varepsilon}A_m^T\eta \\ \dfrac{d\mu}{d\tau} = -\nabla H_{e_P}^T = -W(e_P - \Delta_2) - \dfrac{1}{\varepsilon}A_m^T\mu \end{cases} \quad (31)$$

with the transversality condition $\eta(\tau_f) = 0$ and $\mu(\tau_f) = 0$ since both $e(0)$ and $e_P(0)$ are known.

Taking $\Delta\tilde{K}_x(\tau)$, $\Delta\tilde{K}_r(\tau)$, $\tilde{\Omega}_P(\tau)$, and $\tilde{\Lambda}(\tau)$ as control variables, the necessary conditions are obtained as

$$\begin{cases} \nabla H_{\Delta\tilde{K}_x} = -x\eta^T B_P\hat{\Lambda} \\ \nabla H_{\Delta\tilde{K}_r} = -r\eta^T B_P\hat{\Lambda} \\ \nabla H_{\tilde{\Omega}_P}^T = x\left(\eta^T+\mu^T\right)B_P\hat{\Lambda} \\ \nabla H_{\tilde{\Lambda}} = \left(v+\Omega_P^T(\tau)x\right)\mu^T B_P \end{cases} \tag{32}$$

The BOMAL is expressed by the gradient update laws as

$$\begin{cases} \dfrac{d\Delta K_x^T}{d\tau} = \dfrac{d\Delta\tilde{K}_x^T}{d\tau} = -\Gamma_x\nabla H_{\Delta\tilde{K}_x} = \Gamma_x x\eta^T B_P\hat{\Lambda} \\ \dfrac{d\Delta K_r^T}{d\tau} = \dfrac{d\Delta\tilde{K}_r^T}{d\tau} = -\Gamma_r\nabla H_{\Delta\tilde{K}_r} = \Gamma_r r\eta^T B_P\hat{\Lambda} \\ \dfrac{d\Omega_P}{d\tau} = \dfrac{d\tilde{\Omega}_P}{d\tau} = -\Gamma_{\Omega_P}\nabla H_{\tilde{\Omega}_P}^T = -\Gamma_{\Omega_P}x\left(\eta^T+\mu^T\right)B_P\hat{\Lambda} \\ \dfrac{d\hat{\Lambda}^T}{d\tau} = \dfrac{d\Lambda^T}{d\tau} = -\Gamma_\Lambda\nabla H_{\tilde{\Lambda}} = -\Gamma_\Lambda\left(v+\Omega_P^T(\tau)x\right)\mu^T B_P \end{cases} \tag{33}$$

where $\Gamma_x = \Gamma_x^T > 0 \in R^{n\times n}$, $\Gamma_r = \Gamma_r^T > 0 \in R^{q\times q}$, $\Gamma_{\Omega_P} = \Gamma_{\Omega_P}^T > 0 \in R^{n\times n}$, and $\Gamma_\Lambda = \Gamma_\Lambda^T > 0 \in R^{m\times m}$ are the adaptation rate matrices.

To eliminate $\eta(\tau)$ and $\mu(\tau)$, the following adjoint solutions are assumed by using the sweeping method as

$$\begin{cases} \eta = Pe + S\hat{\Lambda}v \\ \mu = Ue_P + V\hat{\Lambda}\left(v+2\Omega_P^T(\tau)x\right) \end{cases} \tag{34}$$

where $P = P^T > 0$, $U = U^T > 0 \in R^{n\times n}$ and $S, V \in R^{n\times m}$. Substituting (34) into (31) yields

$$\begin{aligned} &P\{\frac{1}{\varepsilon}A_m e - B_P\hat{\Lambda}v + B_P\hat{\Lambda}\left[\left(K_x+\Delta K_x^*\right)x + (K_r+\Delta K_r^*)r \right. \\ &\quad \left. - \Omega_P^{*T}x\right] + B_P\sigma\} + S\frac{d\left(\hat{\Lambda}v\right)}{d\tau} \\ &= -Q(e-\Delta_1) - \frac{1}{\varepsilon}A_m^T\left(Pe+S\hat{\Lambda}v\right) \end{aligned} \tag{35}$$

$$\begin{aligned} &U\Big[\frac{1}{\varepsilon}A_m e_P + B_P\hat{\Lambda}\left(v+2\Omega_P^T(\tau)x\right) - B_P\Lambda(v+\Omega_P^T(\tau)x) \\ &\quad - B_P\hat{\Lambda}\Omega_P^{*T}x + B_P\sigma_P\Big] + V\frac{d\left[\hat{\Lambda}\left(v+2\Omega_P^T(\tau)x\right)\right]}{d\tau} \\ &= -W(e_P-\Delta_2) - \frac{1}{\varepsilon}A_m^T\left[Ue_P + V\hat{\Lambda}\left(v+2\Omega_P^T(\tau)x\right)\right] \end{aligned} \tag{36}$$

Separating (35) that contains $e(\tau)$, $\hat{\Lambda}v$, and the other terms results in

$$\begin{cases} P\dfrac{1}{\varepsilon}A_m + \dfrac{1}{\varepsilon}A_m^T P + Q = 0 \\ \dfrac{1}{\varepsilon}A_m^T S - PB_P = 0 \\ PB_P\hat{\Lambda}\left[\left(K_x+\Delta K_x{}^*\right)x + \left(K_r+\Delta K_r{}^*\right)r - \Omega_P^{*T}x\right] \\ +PB_P\sigma + S\dfrac{d\left(\hat{\Lambda}v\right)}{d\tau} - Q\Delta_1 = 0 \end{cases} \tag{37}$$

with the transversality conditions $P\left(\tau_f\to\infty\right) = 0$ and $S\left(\tau_f\to\infty\right) = 0$.

Separating (36) that contains $e_P(\tau)$, $\hat{\Lambda}\left(v+2\Omega_P^T(\tau)x\right)$, and the other terms results in

$$\begin{cases} U\dfrac{1}{\varepsilon}A_m + \dfrac{1}{\varepsilon}A_m^T U + W = 0 \\ \dfrac{1}{\varepsilon}A_m^T V + UB_P = 0 \\ U\left[-B_P\Lambda\left(v+\Omega_P^T(\tau)x\right) - B_P\hat{\Lambda}\Omega_P^{*T}x + B_P\sigma_P\right] \\ +V\dfrac{d\left[\hat{\Lambda}\left(v+2\Omega_P^T(\tau)x\right)\right]}{d\tau} - W\Delta_2 = 0 \end{cases} \tag{38}$$

with the transversality conditions $U\left(\tau_f\to\infty\right) = 0$ and $V\left(\tau_f\to\infty\right) = 0$.

Therefore, the solutions of P, S, U, and V can be calculated from the following matrix equations

$$\begin{cases} P\dfrac{1}{\varepsilon}A_m + \dfrac{1}{\varepsilon}A_m^T P = -Q \\ S = \varepsilon A_m^{-T}PB_P \\ U\dfrac{1}{\varepsilon}A_m + \dfrac{1}{\varepsilon}A_m^T U = -W \\ V = -\varepsilon A_m^{-T}UB_P \end{cases} \tag{39}$$

To enable the BOMAL has sufficient flexible to compromise between performance and robustness for a control design, we introduce two real modification parameters $\gamma > 0$ and $\kappa > 0$ to permit adjustment of the BOMAL. Then, the solutions of S and V are modified as

$$\begin{cases} S = \gamma\varepsilon A_m^{-T}PB_P \\ V = -\kappa\varepsilon A_m^{-T}UB_P \end{cases} \tag{40}$$

Remark 5: The tracking performance can be traded with robustness by proper selection of γ and κ. Increasing robustness of the adaptive laws to uncertainties by increasing γ and/or κ will decrease the tracking performance, and vice versa.

Then, the adjoint vectors $\eta(\tau)$ and $\mu(\tau)$ are now expressed as

$$\begin{cases} \eta = Pe + \gamma\varepsilon A_m^{-T}PB_P\hat{\Lambda}v \\ \mu = Ue_P - \kappa\varepsilon A_m^{-T}UB_P\hat{\Lambda}\left(v+2\Omega_P^T(\tau)x\right) \end{cases} \tag{41}$$

Substituting (41) into (33) yields the BOMAL in slow time as

$$\begin{cases} \dfrac{d\Delta K_x^T}{d\tau} = \Gamma_x x\left(e^T P + \gamma\varepsilon v^T\hat{\Lambda}^T B_P^T PA_m^{-1}\right)B_P\hat{\Lambda} \\ \dfrac{d\Delta K_r^T}{d\tau} = \Gamma_r r\left(e^T P + \gamma\varepsilon v^T\hat{\Lambda}^T B_P^T PA_m^{-1}\right)B_P\hat{\Lambda} \\ \dfrac{d\Omega_P}{d\tau} = -\Gamma_{\Omega_P}x\Big[e^T P + \gamma\varepsilon v^T\hat{\Lambda}^T B_P^T PA_m^{-1} + e_P^T U \\ -\kappa\varepsilon\left(v+2\Omega_P^T(\tau)x\right)^T\hat{\Lambda}^T B_P^T UA_m^{-1}\Big]B_P\hat{\Lambda} \\ \dfrac{d\hat{\Lambda}^T}{d\tau} = -\Gamma_\Lambda\left(v+\Omega_P^T(\tau)x\right)\Big[e_P^T U \\ -\kappa\varepsilon\left(v+2\Omega_P^T(\tau)x\right)^T\hat{\Lambda}^T B_P^T UA_m^{-1}\Big]B_P \end{cases} \tag{42}$$

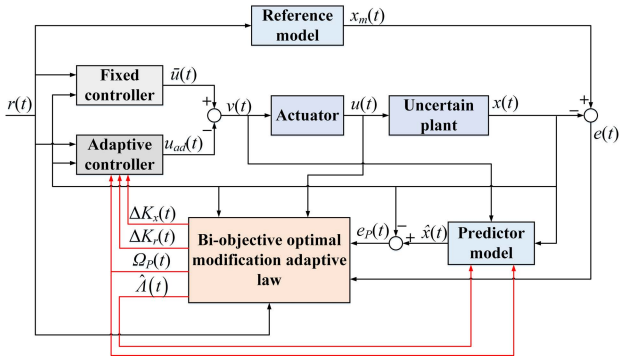

FIGURE 1. Schematic diagram of the bi-objective optimal modification adaptive control system.

Applying the relationship between the slow time τ and the real time t in (4), we obtain the BOMAL in real time as

$$\begin{cases} \Delta\dot{K}_x^T = \varepsilon\Gamma_x x\left(e^T P + \gamma\varepsilon v^T\hat{\Lambda}^T B_P^T P A_m^{-1}\right)B_P\hat{\Lambda} \\ \Delta\dot{K}_r^T = \varepsilon\Gamma_r r\left(e^T P + \gamma\varepsilon v^T\hat{\Lambda}^T B_P^T P A_m^{-1}\right)B_P\hat{\Lambda} \\ \dot{\Omega}_P = -\varepsilon\Gamma_{\Omega_P} x\left[e^T P + \gamma\varepsilon v^T\hat{\Lambda}^T B_P^T P A_m^{-1} + e_P^T U\right. \\ \left. -\kappa\varepsilon\left(v + 2\Omega_P^T x\right)^T\hat{\Lambda}^T B_P^T U A_m^{-1}\right]B_P\hat{\Lambda} \\ \dot{\hat{\Lambda}}^T = -\varepsilon\Gamma_\Lambda\left(v + \Omega_P^T x\right)\left[e_P^T U\right. \\ \left. -\kappa\varepsilon\left(v + 2\Omega_P^T x\right)^T\hat{\Lambda}^T B_P^T U A_m^{-1}\right]B_P \end{cases} \tag{43}$$

Fig. 1 depicts schematic diagram of the bi-objective optimal modification adaptive control system. In Fig. 1, we can see that this adaptive system includes seven subsystems, which are uncertain plant, actuator, reference model, predictor model, fixed controller, adaptive controller, and BOMAL. The BOMAL combines with the fixed and adaptive controller together ensure robustness of the system with matched uncertainty and SAD. Now, we need to prove that the proposed BOMAL is stable and results in uniformly bounded tracking error.

Lemma 2 [14]: For any vectors $\phi, \varphi \in \mathbb{R}^n$, the following trace property satisfies

$$trace\left(\phi\varphi^T\right) = \varphi^T\phi \tag{44}$$

Lemma 3 [14]: For any square real matrix $\Pi \in \mathbb{R}^{n\times n}$, it can be decomposed into a symmetric part N and anti-symmetric part O as

$$\Pi = N + O \tag{45}$$

where $N = N^T = \frac{1}{2}\left(\Pi + \Pi^T\right)$, $O = -O^T = \frac{1}{2}\left(\Pi - \Pi^T\right)$.

For any arbitrary vector $\alpha \in \mathbb{R}^n$, then

$$\alpha^T\Pi\alpha = \alpha^T N\alpha \tag{46}$$

Theorem 1: For the linear plant in (1) and subject to SAD, the BOMAL in (43) is stable and results in uniformly bounded tracking error and predictor error.

The proof can be found in Appendix A.

IV. TURBOFAN ENGINE APPLICATION

The proposed BOMAL is applied to a turbofan engine with SAD. The nonlinear model of this turbofan engine is a component-based model established by using MATLAB and the Simulink toolbox for the modeling and analysis of thermodynamic system [29]. All the modeling data is provided by gas turbine simulation program [30]. This nonlinear model, which has been used in other studies [30]–[34], is the foundation of the following control design and simulation analysis.

A. BI-OBJECTIVE OPTIMAL MODIFICATION ADAPTIVE CONTROL DESIGN

Under the standard day sea level condition (SLC), we take the full thrust state (FTS) (N_f = 10065 r/min, N_c = 12832 r/min) as an example to design the bi-objective optimal modification adaptive controller (BOMAC). For the convenience of controller design, all the variables are normalized: $x_1(t) = N_f(t)/N_{fd}$ denotes the normalized fan speed, and N_{fd} = 10065 r/min denotes the design value; $x_2(t) = N_c(t)/N_{cd}$ denotes the normalized core speed, and N_{cd} = 12832 r/min denotes the design value; $u_1(t) = W_f(t)/W_{fd}$ denotes the normalized fuel flow rate, and W_{fd} = 1.144 kg/s denotes the design value; $u_2(t) = A_8(t)/A_{8d}$ denotes the normalized throat area of nozzle, and A_{8d} = 0.298058 m^2 denotes the design value. Then the linearized model is

$$\begin{bmatrix}\delta\dot{x}_1\\ \delta\dot{x}_2\end{bmatrix} = \begin{bmatrix}-6.5499 & 5.5686\\ 0.1298 & -3.7204\end{bmatrix}\begin{bmatrix}\delta x_1\\ \delta x_2\end{bmatrix} + \begin{bmatrix}0.4829 & 1.9816\\ 0.6643 & -0.01428\end{bmatrix}\begin{bmatrix}\delta u_1\\ \delta u_2\end{bmatrix} \tag{47}$$

where $\delta x = x - x_e$, $\delta u = u - u_e$; x_e and u_e are normalized equilibrium values at the design point.

Because of the influence of degradation, the controller is subject to SAD

$$\begin{bmatrix}\delta\dot{u}_1\\ \delta\dot{u}_2\end{bmatrix} = 0.1\begin{bmatrix}-20 & 0\\ 0 & -20\end{bmatrix}(\delta u - \delta v) \tag{48}$$

Then, according to the performance requirements of the turbofan engine, the closed-loop dynamics of the turbofan engine is required to have the characteristics of first order function with time constant equal to 0.1s. Thus, we obtain the reference model as

$$\begin{bmatrix}\delta\dot{x}_{m1}\\ \delta\dot{x}_{m2}\end{bmatrix} = \begin{bmatrix}-10 & 0\\ 0 & -10\end{bmatrix}\begin{bmatrix}\delta x_{m1}\\ \delta x_{m2}\end{bmatrix} + \begin{bmatrix}10 & 0\\ 0 & 10\end{bmatrix}\begin{bmatrix}\delta r_1\\ \delta r_2\end{bmatrix} \tag{49}$$

Based on (16), we obtain the reduced-order system matrices as

$$A_P = \begin{bmatrix}-20.0000 & 7.1054\times10^{-15}\\ -1.1102\times10^{-16} & -20.0000\end{bmatrix}$$

$$B_P = \begin{bmatrix}4.6485 & 6.1684\\ 3.7333 & 0.1384\end{bmatrix}$$

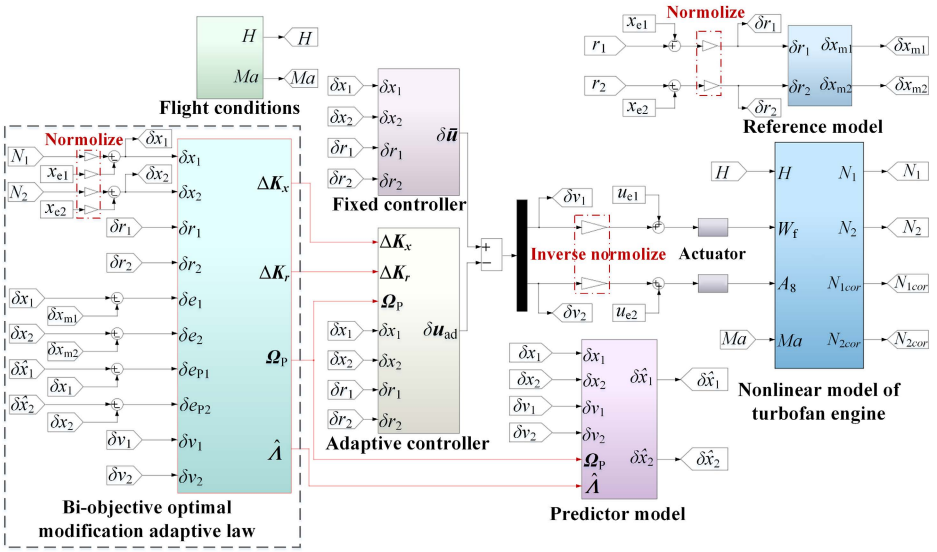

FIGURE 2. Turbofan engine simulation platform.

According to the ideal model matching conditions in (19), we obtain

$$K_x = \begin{bmatrix} -0.232 & -9.464 \\ -1.685 & -0.504 \end{bmatrix},\ K_r = \begin{bmatrix} 0.108 & 14.975 \\ 5.020 & -3.649 \end{bmatrix}$$

Let $Q = 10I$ and $W = 1850I$, then the solution of (39) yields

$$P = \begin{bmatrix} 0.05 & 0 \\ 0 & 0.05 \end{bmatrix},\ U = \begin{bmatrix} 9.25 & 0 \\ 0 & 9.25 \end{bmatrix}$$

Then, we properly choose the adaption rate matrices Γ_x, Γ_r, Γ_{Ω_P}, and Γ_Λ, and the modification parameters γ and κ as

$$\Gamma_x = \begin{bmatrix} 100 & 0 \\ 0 & 100 \end{bmatrix},\ \Gamma_r = \begin{bmatrix} 100 & 0 \\ 0 & 100 \end{bmatrix},\ \gamma = 0.005$$
$$\Gamma_{\Omega_P} = \begin{bmatrix} 1000 & 0 \\ 0 & 50 \end{bmatrix},\ \Gamma_\Lambda = \begin{bmatrix} 45 & 0 \\ 0 & 673 \end{bmatrix},\ \kappa = 0.005$$

Applying the BOMAL in (43), the weight update laws are given by

$$\begin{cases} \Delta\dot{K}_x^T = \varepsilon\Gamma_x\delta x\left(\delta e^T P + \gamma\varepsilon\delta v^T\hat{\Lambda}^T B_P^T P A_m^{-1}\right)B_P\hat{\Lambda} \\ \Delta\dot{K}_r^T = \varepsilon\Gamma_r\delta r\left(\delta e^T P + \gamma\varepsilon\delta v^T\hat{\Lambda}^T B_P^T P A_m^{-1}\right)B_P\hat{\Lambda} \\ \dot{\Omega}_P = -\varepsilon\Gamma_{\Omega_P}\delta x\left[\delta e^T P + \gamma\varepsilon\delta v^T\hat{\Lambda}^T B_P^T P A_m^{-1} + \delta e_P^T U\right. \\ \left.-\kappa\varepsilon\left(\delta v + 2\Omega_P^T\delta x\right)^T\hat{\Lambda}^T B_P^T U A_m^{-1}\right]B_P\hat{\Lambda} \\ \dot{\hat{\Lambda}}^T = -\varepsilon\Gamma_\Lambda\left(\delta v + \Omega_P^T\delta x\right)\left[\delta e_P^T U\right. \\ \left.-\kappa\varepsilon\left(\delta v + 2\Omega_P^T\delta x\right)^T\hat{\Lambda}^T B_P^T U A_m^{-1}\right]B_P \end{cases} \tag{50}$$

B. SIMULATION RESULTS

A series of simulations are conducted as illustrated in Fig. 2 to verify the effectiveness and superiority of the designed BOMAC. Firstly, a typical turbofan engine control mission is used to verify the robust performance of the BOMAC. Then,

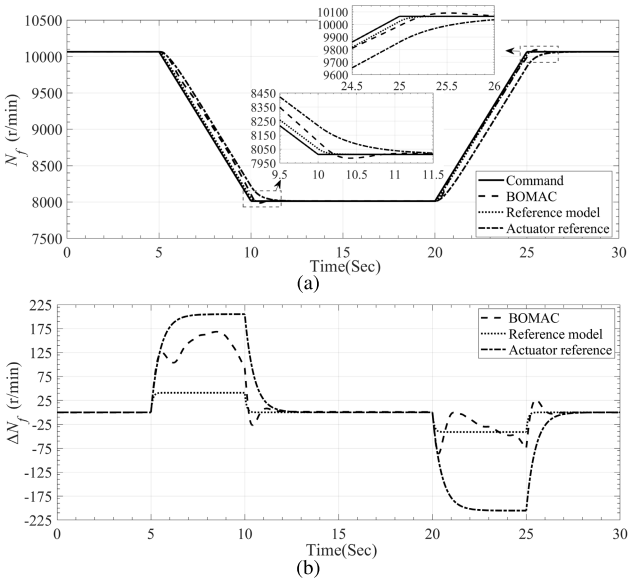

FIGURE 3. (a) Simulation result of fan speed N_f at SLC; (b) Fan speed difference ΔN_f between the response and the command of N_f.

the robust performance of the BOMAC is verified by the same engine control mission at flight conditions $Ma = 0.5$, $H = 5$ km and $Ma = 1.0, H = 10$ km. Finally, the superiority of the BOMAC is benchmarked with an LMI optimization gain scheduled controller (LMI-OGSC) [6] and a μ synthesis controller [34].

1) ROBUST PERFORMANCE VERIFICATION AT SLC

Based on the simulation platform in Fig. 2, the robust performance of the designed BOMAC at SLC is verified through simulation analysis.

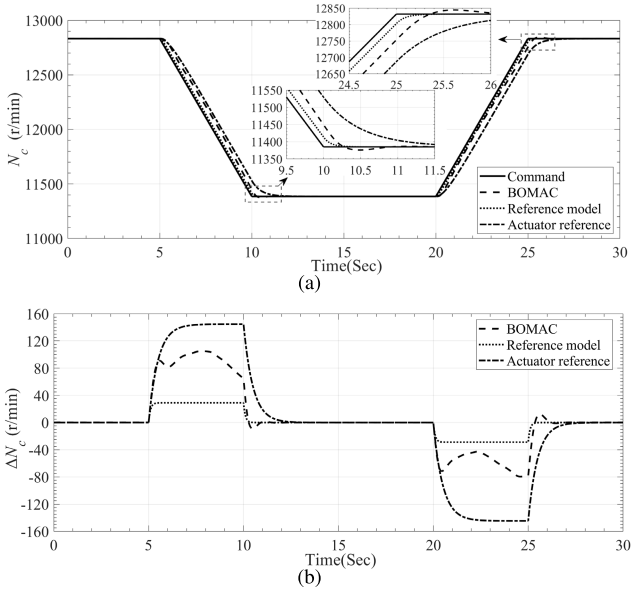

FIGURE 4. (a) Simulation result of core speed N_c at SLC; (b) Core speed difference ΔN_c between the response and the command of N_c.

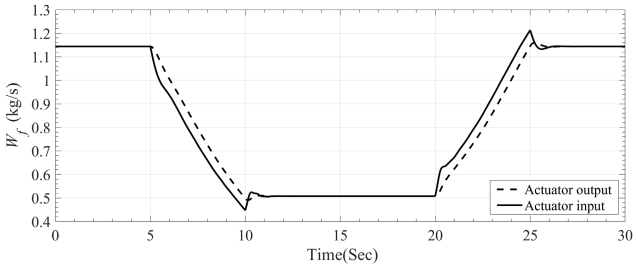

FIGURE 5. Regulating process of fuel flow rate W_f at SLC.

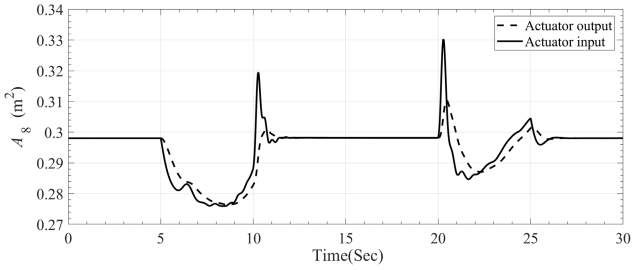

FIGURE 6. Regulating process of throat area A_8 at SLC.

Fig. 3 gives the simulation result of fan speed, including: (a) the fan speed N_f and (b) the fan speed difference ΔN_f between the response and the command of N_f. In Fig. 3 (a), the black line represents the command of N_f, the dashed line represents the response of N_f controlled by the BOMAC, the dotted line represents the response of N_f of the reference model, and the dash-dot line represents the response of N_f of the actuator reference (According to (48), we use SAD as a reference model to generate a baseline response of the command signal when the closed-loop dynamics of the turbofan engine is with SAD). In Fig. 3 (b), the dashed line represents the ΔN_f of the BOMAC, the dotted line represents the ΔN_f of the reference model, and the dash-dot line represents the ΔN_f of the actuator reference. The plot color coding will also apply to the later result figures. As seen in Fig. 3 (a), the response of N_f under the control of the BOMAC can track the command even though with SAD and is better than the response of N_f of the actuator reference, which means the BOMAC has compensated the negative influence of SAD. As shown in Fig. 3, the steady-state error is less than 0.01%, the maximum dynamic error is less than 2% at around 8s, and the maximum overshoot is less than 0.32% at around 10.5s, which means the designed BOMAC has good robust performance on N_f control at SLC.

As we can see from Fig. 4 (a), the response of N_c under the control of the BOMAC can also track the command signal with SAD and is better than the response of N_c of the actuator reference. As can be seen from Fig. 4, the steady-state error is less than 0.01%, the maximum dynamic error is less than 1% at around 8s, and the maximum overshoot is less than 0.15% at around 25.5s.

Fig. 5 shows the regulating process of the fuel flow rate at SLC. From Fig. 5, the designed BOMAC regulates the fuel flow rate command changing faster to compensate the negative influence of SAD to achieve good control performance of the engine. Fig. 6 illustrates histories of the throat area at SLC. As can be seen from Fig. 6, the throat area command is changed fast in transient process to compensate the negative influence of SAD to ensure good control performance of the engine.

Fig. 7 shows the histories of $\|e\|_2$, $\|e_P\|_2$, $\|\Delta K_x\|_2$, $\|\Delta K_r\|_2$, $\|\Omega_P\|_2$, and $\left\|\hat{\Lambda}\right\|_2$ during the engine regulation at SLC. As can be seen from Fig. 7, e, e_P, ΔK_x, ΔK_r, Ω_P, and $\hat{\Lambda}$ all are bounded, which verifies the validity of Theorem 1 in simulation.

2) ROBUST PERFORMANCE VERIFICATION AT HIGH-ALTITUDE FLIGHT CONDITIONS

At high-altitude flight conditions $Ma = 0.5$, $H = 5$ km and $Ma = 1.0$, $H = 10$ km, we use the same simulation platform, controller parameters, and engine process (FTS $\rightarrow$ idle $\rightarrow$ FTS) as in SLC verification to conduct simulation to further verify the robustness of the designed BOMAC respectively.

The simulation results of fan speed at $Ma = 0.5$, $H = 5$ km and $Ma = 1.0$, $H = 10$ km are shown in Fig. 8 and Fig. 9 respectively. As can be seen from Fig. 8 and Fig. 9, the steady-state error is less than 0.01%, the maximum dynamic error is less than 3% at around 5.5s, and the maximum overshoot is no larger than 0.4% at around 10.5s, which means the designed BOMAC has good robust performance on N_f control at both $Ma = 0.5$, $H = 5$ km and $Ma = 1.0$, $H = 10$ km.

Fig. 10 and Fig. 11 give the simulation results of core speed at at $Ma = 0.5$, $H = 5$ km and $Ma = 1.0$, $H = 10$ km respectively. As we can see from Fig. 10 and Fig. 11, the steady-state error is less than 0.01%, the maximum dynamic

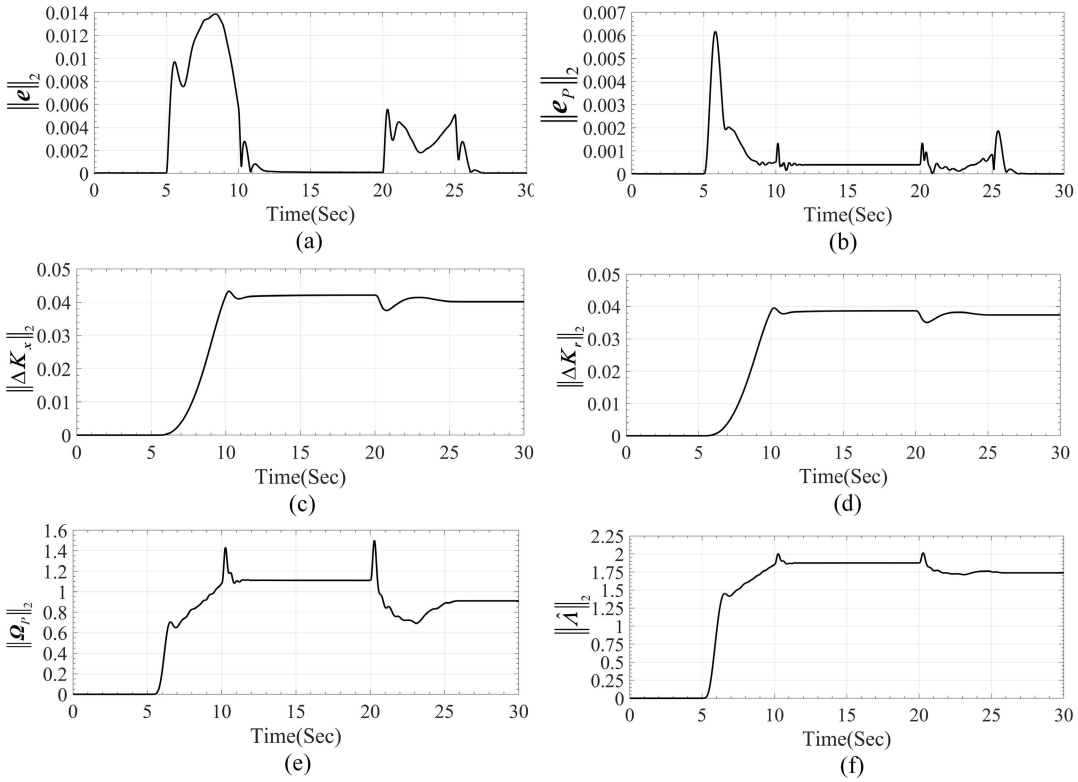

FIGURE 7. (a) $\|e\|_2$; (b) $\|e_P\|_2$; (c) $\|\Delta K_x\|_2$; (d) $\|\Delta K_r\|_2$; (e) $\|\Omega_P\|_2$; (f) $\left\|\hat{\Lambda}\right\|_2$.

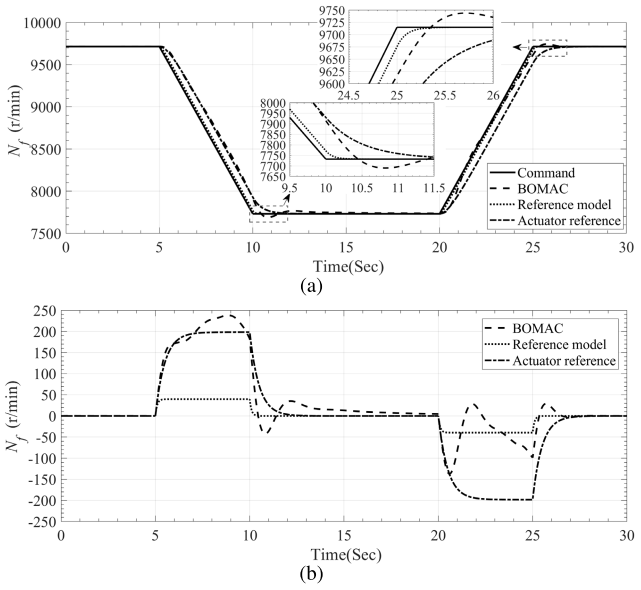

FIGURE 8. (a) Simulation result of fan speed N_f at $Ma = 0.5$, $H = 5$ km; (b) ΔN_f.

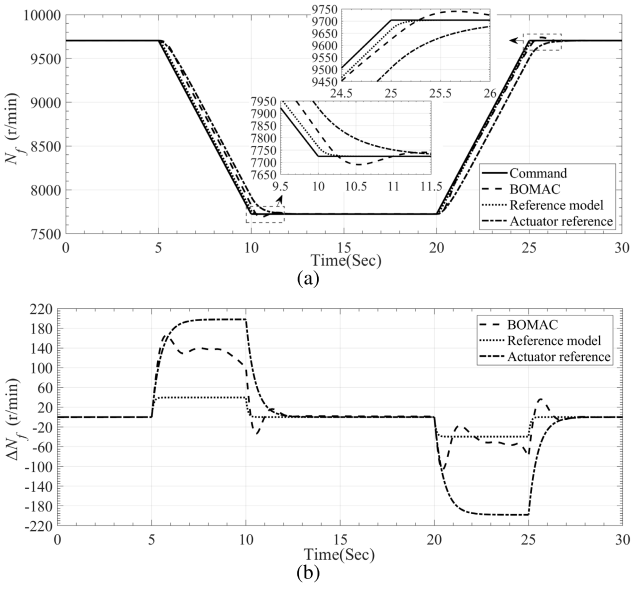

FIGURE 9. (a) Simulation result of fan speed N_f at $Ma = 1.0$, $H = 10$ km; (b) ΔN_f.

error is no larger than 1.5% at around 8s, and the maximum overshoot is less than 0.15% at around 10.5s.

Fig. 12 and Fig. 13 illustrate the regulating process of the fuel flow rate at $Ma = 0.5$, $H = 5$ km and $Ma = 1.0$, $H = 10$ km respectively. From Fig. 12 and Fig. 13, the designed BOMAC controls the fuel flow rate command changing faster to compensate the negative influence of SAD to achieve good control performance of the engine. Fig. 14 and Fig. 15 show the regulating process of the throat area at $Ma = 0.5$, $H = 5$ km and $Ma = 1.0$, $H = 10$ km respectively. As we

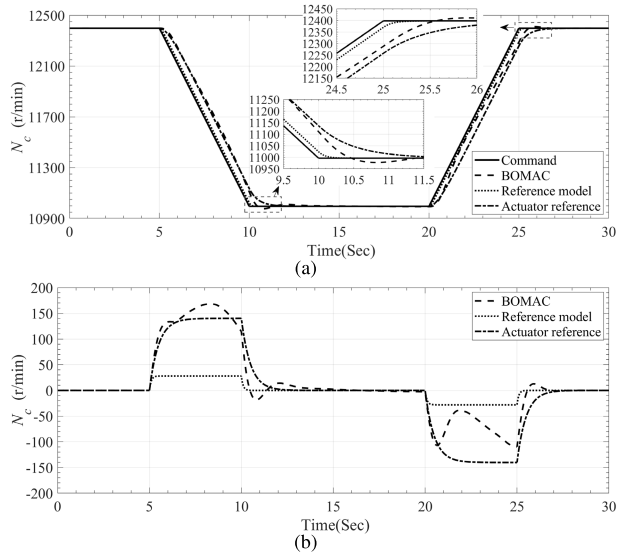

FIGURE 10. (a) Simulation result of core speed N_c at $Ma = 0.5$, $H = 5$ km; (b) ΔN_c.

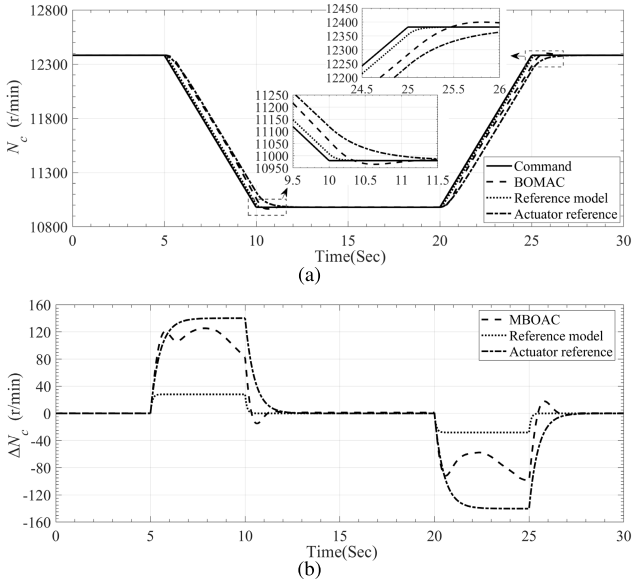

FIGURE 11. (a) Simulation result of core speed N_c at $Ma = 1.0$, $H = 10$ km; (b) ΔN_c.

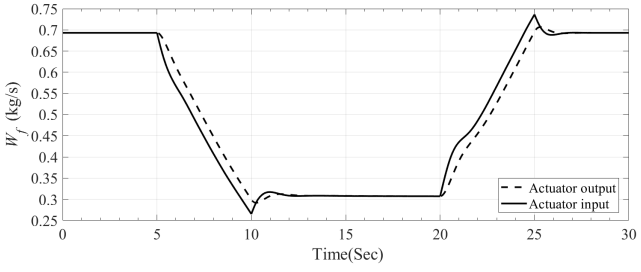

FIGURE 12. Regulating process of W_f at $Ma = 0.5$, $H = 5$ km.

can see from Fig. 14 and Fig. 15, the throat area command is changed fast in transient process to compensate the

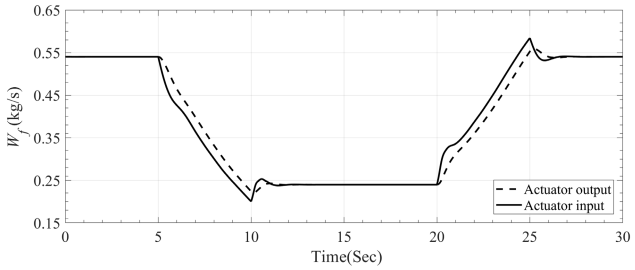

FIGURE 13. Regulating process of W_f at $Ma = 1.0$, $H = 10$ km.

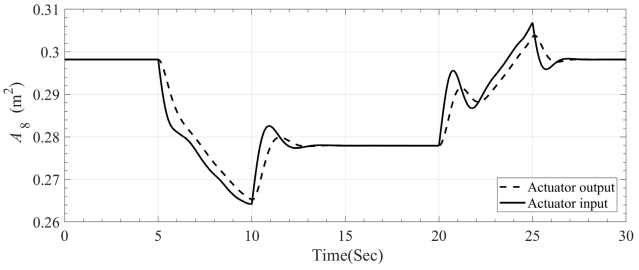

FIGURE 14. Regulating process of A_8 at $Ma = 0.5$, $H = 5$ km.

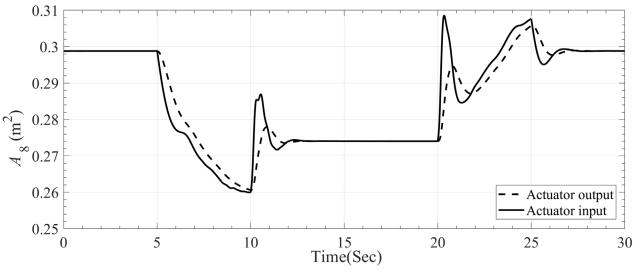

FIGURE 15. Regulating process of A_8 at $Ma = 1.0$, $H = 10$ km.

influence of SAD to ensure good control performance of the engine.

Fig. 16 and Fig. 17 illustrate the histories of $\|e\|_2$, $\|e_P\|_2$, $\|\Delta K_x\|_2$, $\|\Delta K_r\|_2$, $\|\Omega_P\|_2$, and $\left\|\hat{\Lambda}\right\|_2$ during the engine regulation at $Ma = 0.5$, $H = 5$ km and $Ma = 1.0$, $H = 10$ km respectively. As can be seen from Fig. 16 and Fig. 17, e, e_P, ΔK_x, ΔK_r, Ω_P, and $\hat{\Lambda}$ all are bounded, which further verifies the validity of Theorem 1 in simulation.

3) COMPARISON VERIFICATION

The simulation results of the BOMAC are compared with the simulation results of an LMI-OGSC [5] and a μ synthesis controller [33], [34] to verify the superiority of the BOMAC.

Fig. 18 illustrates the comparison result of fan speed, including: (a) the fan speed N_f and (b) the fan speed difference ΔN_f. As can be seen From Fig. 18, the biggest dynamic errors of the LMI-OGSC and the μ synthesis controller are almost two times of that of the BOMAC; the LMI-OGSC has big overshoot at around 10s and 27s and its settling time is about 4s; although the μ synthesis controller

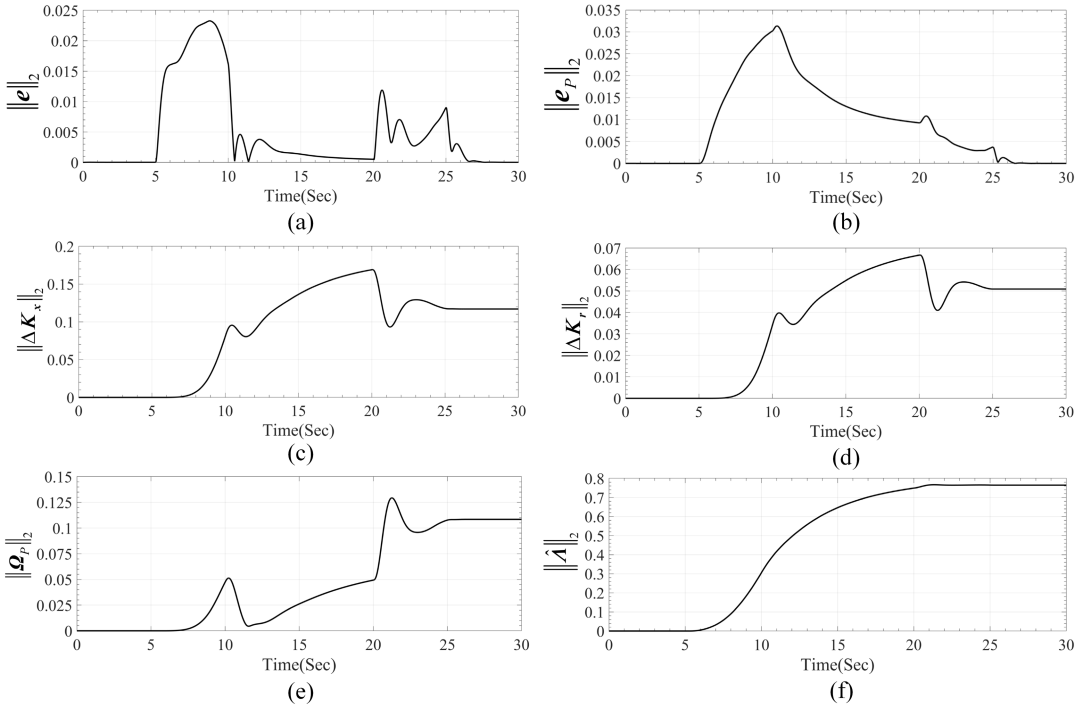

FIGURE 16. (a) $\|e\|_2$; (b) $\|e_P\|_2$; (c) $\|\Delta K_x\|_2$; (d) $\|\Delta K_r\|_2$; (e) $\|\Omega_P\|_2$; (f) $\left\|\hat{\Lambda}\right\|_2$ at $Ma = 0.5$, $H = 5$ km.

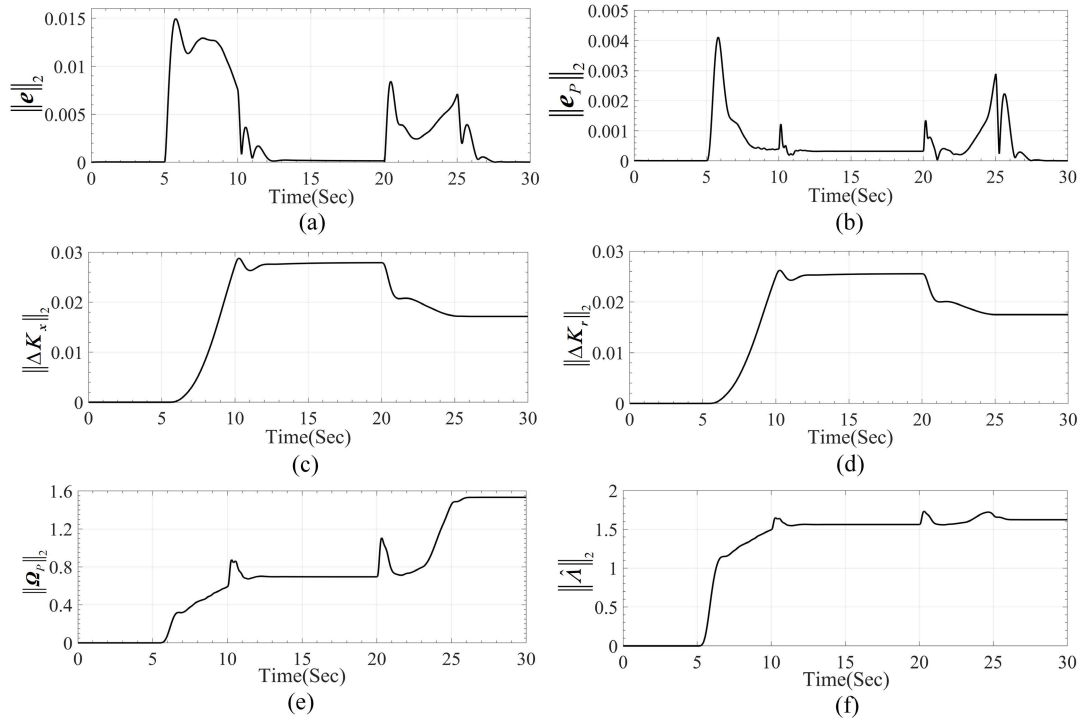

FIGURE 17. (a) $\|e\|_2$; (b) $\|e_P\|_2$; (c) $\|\Delta K_x\|_2$; (d) $\|\Delta K_r\|_2$; (e) $\|\Omega_P\|_2$; (f) $\left\|\hat{\Lambda}\right\|_2$ at $Ma = 1.0$, $H = 10$ km.

has small overshoot, it has a longer settling time compared with the BOMAC. Table 1 is the comparison table of the control performance indices of the three controllers on N_f control. From Table 1, for these three control performance indices, the BOMAC has smaller values than the other two controllers do, which means the designed BOMAC clearly

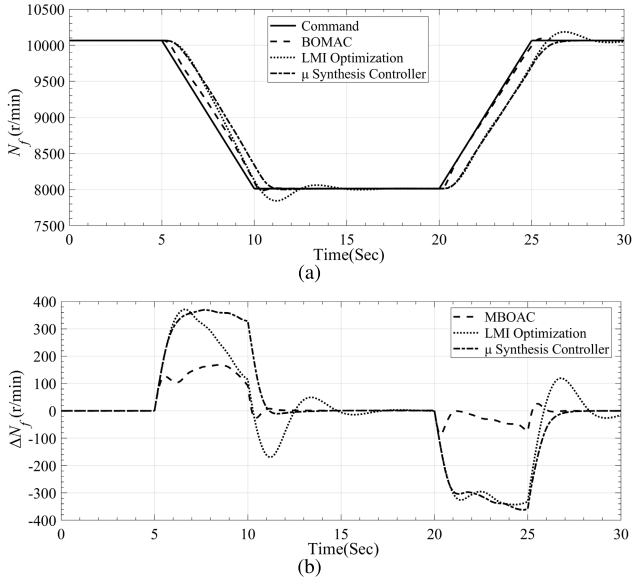

FIGURE 18. (a) Comparison results of fan speed N_f; (b) ΔN_f.

TABLE 1. Comparison table of the control performance indices of the three controllers on N_f.

Controller	MAE	RMSE	ITAE
BOMAC	29.96	58.98	898.95
LMI-OGSC	113.51	172.58	3406.31
μ synthesis controller	114.82	189.43	3445.84

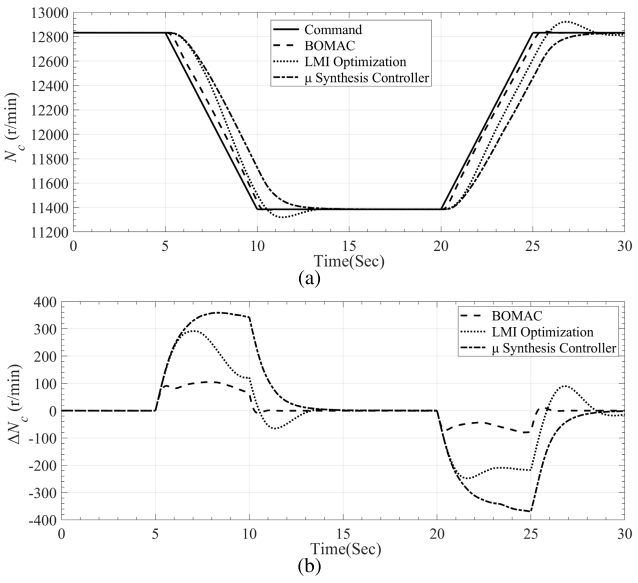

FIGURE 19. (a) Comparison result of core speed N_c; (b) ΔN_c.

provides better performance on N_f control than the other two controllers do.

Fig. 19 depicts the comparison result of core speed, including: (a) the core speed N_c and (b) the rotation speed difference ΔN_c. As can be seen from Fig. 19, the designed BOMAC also clearly provides better performance on N_c control than the other two controllers do. The comparison table of the control performance indices of the three controllers on N_c control is shown in Table 2. According to the above analysis, at both SLC and high-altitude condition, the designed BOMAC can achieve good robust performance of the turbofan engine with SAD, and provides better performance than the LMI-OGSC and the μ synthesis controller do.

TABLE 2. Comparison table of the control performance indices of the three controllers on N_c.

Controller	MAE	RMSE	ITAE
BOMAC	25.44	44.44	763.36
LMI-OGSC	80.59	126.66	2418.37
μ synthesis controller	118.84	187.64	3566.36

V. CONCLUSION

A bi-objective optimal modification adaptive control method is proposed for turbofan engines with SAD and matched uncertainty. In the proposed method, a singular perturbation approach is introduced to transform the plant and actuator dynamics into a reduced-order system with slow time coordinate, and the bi-objective optimal modification adaptive law is deduced based on the reduced-order system.

The proposed adaptive control method is applied to a turbofan engine with SAD. At both SLC and high-altitude condition, the efficiency of the designed BOMAC is demonstrated by a regulation mission of controlling the engine from FTS to idle and back to FTS. The simulation results show that the BOMAC achieved a good robust performance on both fan and core speed control at both SLC and high-altitude condition with SAD. For fan speed control, the steady-state error, the dynamic error, and the maximum overshoot at both SLC and high-altitude condition are less than 0.01%, 2%, and 0.4%, respectively. For core speed control, the steady-state error, the dynamic error, and the maximum overshoot at both SLC and high-altitude condition are less than 0.01%, 1%, and 0.15%, respectively. Additionally, through comparing with the LMI-OGSC and μ synthesis controller, the designed BOMAC clearly provides better performance than the other two controllers do.

In future work, the proposed method will be applied for robust control of turbofan engines over the whole working envelope. In addition, the proposed BOMAC will be verified in semi-physical and full physical simulation.

APPENDIX A
PROOF OF THEOREM 1

Proof: Choose a Lyapunov candidate function

$$\begin{aligned} V\left(e,\ e_P,\ \Delta\tilde{K}_x,\ \Delta\tilde{K}_r,\ \tilde{\Omega}_P,\ \tilde{\Lambda}\right) &= e^T Pe + e_P^T U e_P + trace\left(\Delta\tilde{K}_x\Gamma_x^{-1}\Delta\tilde{K}_x^T\right) \\ &+ trace\left(\Delta\tilde{K}_r\Gamma_r^{-1}\Delta\tilde{K}_r^T\right) + trace\left(\tilde{\Omega}_P^T\Gamma_{\Omega_P}^{-1}\tilde{\Omega}_P\right) \\ &+ trace\left(\tilde{\Lambda}\Gamma_\Lambda^{-1}\tilde{\Lambda}^T\right) \end{aligned} \quad (51)$$

Differentiating $V\left(e,\ e_P,\ \Delta\tilde{K}_x,\ \Delta\tilde{K}_r,\ \tilde{\Omega}_P,\ \tilde{\Lambda}\right)$ in slow time yields

$$\begin{aligned}
&\frac{dV\left(e,\ e_P,\ \Delta\tilde{K}_x,\ \Delta\tilde{K}_r,\ \tilde{\Omega}_P,\ \tilde{\Lambda}\right)}{d\tau}\\
&=-e^TQe-2e^TPB_P\hat{\Lambda}(\Delta\tilde{K}_xx+\Delta\tilde{K}_rr-\tilde{\Omega}_P^Tx)+2e^TPB_P\sigma\\
&\quad-e_P^TWe_P+2e_P^TUB_P\tilde{\Lambda}(v+\Omega_P^Tx)+2e_P^TUB_P\hat{\Lambda}\tilde{\Omega}_P^Tx\\
&\quad+2e_P^TUB_P\sigma_P+2trace\left[\Delta\tilde{K}_xx\left(e^TP+\gamma\varepsilon v^T\hat{\Lambda}^TB_P^TPA_m^{-1}\right)B_P\hat{\Lambda}\right]\\
&\quad+2trace\left[\Delta\tilde{K}_rr(e^TP+\gamma\varepsilon v^T\hat{\Lambda}^TB_P^TPA_m^{-1})B_P\hat{\Lambda}\right]\\
&\quad+2trace\left\{-\tilde{\Omega}_P^Tx\left[e^TP+\gamma\varepsilon v^T\hat{\Lambda}^TB_P^TPA_m^{-1}+e_P^TU\right.\right.\\
&\quad\left.\left.-\kappa\varepsilon\left(v+2\Omega_P^Tx\right)^T\hat{\Lambda}^TB_P^TUA_m^{-1}\right]B_P\hat{\Lambda}\right\}\\
&\quad+2trace\left\{-\tilde{\Lambda}\left(v+\Omega_P^Tx\right)\left[e_P^TU\right.\right.\\
&\quad\left.\left.-\kappa\varepsilon\left(v+2\Omega_P^Tx\right)^T\hat{\Lambda}^TB_P^TUA_m^{-1}\right]B_P\right\}
\end{aligned}\tag{52}$$

According to the Lemma 2, we have

$$\begin{aligned}
&\frac{dV\left(e,\ e_P,\ \Delta\tilde{K}_x,\ \Delta\tilde{K}_r,\ \tilde{\Omega}_P,\ \tilde{\Lambda}\right)}{d\tau}\\
&=-e^TQe+2e^TPB_P\sigma-e_P^TWe_P+2e_P^TUB_P\sigma_P\\
&\quad+2\gamma\varepsilon v^T\hat{\Lambda}^TB_P^TPA_m^{-1}B_P\hat{\Lambda}\Delta\tilde{K}_xx\\
&\quad+2\gamma\varepsilon v^T\hat{\Lambda}^TB_P^TPA_m^{-1}B_P\hat{\Lambda}\Delta\tilde{K}_rr\\
&\quad-2\gamma\varepsilon v^T\hat{\Lambda}^TB_P^TPA_m^{-1}B_P\hat{\Lambda}\tilde{\Omega}_P^Tx\\
&\quad+2\kappa\varepsilon\left(v+2\Omega_P^Tx\right)^T\hat{\Lambda}^TB_P^TUA_m^{-1}B_P\hat{\Lambda}\tilde{\Omega}_P^Tx\\
&\quad+2\kappa\varepsilon\left(v+2\Omega_P^Tx\right)^T\hat{\Lambda}^TB_P^TUA_m^{-1}B_P\tilde{\Lambda}\left(v+\Omega_P^Tx\right)
\end{aligned}\tag{53}$$

Let

$$\begin{cases}
\tilde{v}=\Delta\tilde{K}_xx+\Delta\tilde{K}_rr-\tilde{\Omega}_P^Tx\\
v^*=\bar{u}+\Delta K_x^*x+\Delta K_x^*r-\Omega_P^{*T}x\\
\theta=\begin{bmatrix}x\\ v+\Omega_P^Tx\end{bmatrix}\\
\Xi=\begin{bmatrix}\Omega_P\hat{\Lambda}^T & 0\\ 0 & \hat{\Lambda}^T\end{bmatrix}\\
\Xi^*=\begin{bmatrix}\Omega_P^* & 0\\ 0 & \Lambda^T\end{bmatrix}\\
\tilde{\Xi}=\Xi-\Xi^*\\
\bar{B}_P=\begin{bmatrix}B_P & B_P\end{bmatrix}
\end{cases}\tag{54}$$

Then, (53) becomes

$$\begin{aligned}
&\frac{dV\left(e,\ e_P,\ \tilde{\Theta},\ \tilde{\Xi}\right)}{d\tau}\\
&=-e^TQe+2e^TPB_P\sigma-e_P^TWe_P+2e_P^TUB_P\sigma_P\\
&\quad+2\gamma\varepsilon\tilde{v}^T\hat{\Lambda}^TB_P^TPA_m^{-1}B_P\hat{\Lambda}\tilde{v}+2\gamma\varepsilon v^{*T}\hat{\Lambda}^TB_P^TPA_m^{-1}B_P\hat{\Lambda}\tilde{v}\\
&\quad+2\kappa\varepsilon\theta^T\tilde{\Xi}\bar{B}_P^TUA_m^{-1}\bar{B}_P\tilde{\Xi}^T\theta\\
&\quad+2\kappa\varepsilon\theta^T\Xi^*\bar{B}_P^TUA_m^{-1}\bar{B}_P\tilde{\Xi}^T\theta
\end{aligned}\tag{55}$$

According to the Lemma 3, we have

$$\begin{aligned}
2\tilde{v}^T\hat{\Lambda}^TB_P^TPA_m^{-1}B_P\hat{\Lambda}\tilde{v}&=-\varepsilon\tilde{v}^T\hat{\Lambda}^TB_P^TA_m^{-T}QA_m^{-1}B_P\hat{\Lambda}\tilde{v}\\
2\theta^T\tilde{\Xi}\bar{B}_P^TUA_m^{-1}\bar{B}_P\tilde{\Xi}^T\theta&=-\varepsilon\theta^T\tilde{\Xi}\bar{B}_P^TA_m^{-T}WA_m^{-1}\bar{B}_P\tilde{\Xi}^T\theta
\end{aligned}$$

Let

$$\begin{cases}
\tilde{\Theta}=\left[\Delta\tilde{K}_x-\tilde{\Omega}_P^T\ \ \Delta\tilde{K}_r\right]\\
\Theta^*=\left[K_x+\Delta K_x^*-\Omega_P^{*T}\ \ K_r+\Delta K_r^*\right]
\end{cases}\tag{56}$$

Then, (55) is bounded by

$$\begin{aligned}
&\frac{dV\left(e,\ e_P,\ \tilde{\Theta},\ \tilde{\Xi}\right)}{d\tau}\\
&\le-\lambda_{min}(Q)\|e\|^2+2\|e\|\|PB_P\|\sigma_0-\lambda_{min}(W)\|e_P\|^2\\
&\quad+2\|e_P\|\|UB_P\|\sigma_{P0}\\
&\quad-\gamma\varepsilon^2\lambda_{min}(B_P^TA_m^{-T}QA_m^{-1}B_P)\|\Phi(x,\ r)\|^2\left\|\hat{\Lambda}\right\|^2\left\|\tilde{\Theta}\right\|^2\\
&\quad+2\gamma\varepsilon\|\Phi(x,\ r)\|^2\left\|B_P^TPA_m^{-1}B_P\right\|\left\|\hat{\Lambda}\right\|^2\left\|\tilde{\Theta}\right\|\Theta_0\\
&\quad-\kappa\varepsilon^2\lambda_{min}(\bar{B}_P^TA_m^{-T}WA_m^{-1}\bar{B}_P)\|\theta\|^2\left\|\tilde{\Xi}\right\|^2\\
&\quad+2\kappa\varepsilon\|\theta\|^2\left\|\bar{B}_P^TUA_m^{-1}\bar{B}_P\right\|\left\|\tilde{\Xi}\right\|\Xi_0
\end{aligned}\tag{57}$$

where $\Theta_0=sup\|\Theta^*\|$, $\Xi_0=sup\|\Xi^*\|$, and λ denotes the eigenvalue.

Let

$$\begin{cases}
z_1=\lambda_{min}(Q)\\
z_2=\|PB_P\|\sigma_0/z_1\\
z_3=\lambda_{min}(W)\\
z_4=\|UB_P\|\sigma_{P0}/z_3\\
z_5=\lambda_{min}\left(B_P^TA_m^{-T}QA_m^{-1}B_P\right)\|\Phi(x,\ r)\|^2\left\|\hat{\Lambda}\right\|^2\\
z_6=\left\|B_P^TPA_m^{-1}B_P\right\|\Theta_0/\lambda_{min}\left(B_P^TA_m^{-T}QA_m^{-1}B_P\right)\\
z_7=\lambda_{min}\left(\bar{B}_P^TA_m^{-T}WA_m^{-1}\bar{B}_P\right)\|\theta\|^2\\
z_8=\left\|\bar{B}_P^TUA_m^{-1}\bar{B}_P\right\|\Xi_0/\lambda_{min}\left(\bar{B}_P^TA_m^{-T}WA_m^{-1}\bar{B}_P\right)
\end{cases}\tag{58}$$

Through substituting (58) into (57), we obtain

$$\begin{aligned}
&\frac{dV\left(e,\ e_P,\ \tilde{\Theta},\ \tilde{\Xi}\right)}{d\tau}\\
&\le-z_1(\|e\|-z_2)^2+z_1z_2^2-z_3(\|e_P\|-z_4)^2+z_3z_4^2\\
&\quad-\gamma z_5(\varepsilon\left\|\tilde{\Theta}\right\|-z_6)^2+\gamma z_5z_6^2-\kappa z_7(\varepsilon\left\|\tilde{\Xi}\right\|-z_8)^2+\kappa z_7z_8^2
\end{aligned}\tag{59}$$

Through applying the relationship between the slow time τ and the real time t in (4), we obtain the derivative of Lyapunov candidate function in real time as

$$\begin{aligned}
&\dot{V}\left(e,\ e_P,\ \tilde{\Theta},\ \tilde{\Xi}\right)\\
&\le-\varepsilon z_1(\|e\|-z_2)^2+\varepsilon z_1z_2^2-\varepsilon z_3(\|e_P\|-z_4)^2+\varepsilon z_3z_4^2\\
&\quad-\gamma\varepsilon z_5(\varepsilon\left\|\tilde{\Theta}\right\|-z_6)^2+\gamma\varepsilon z_5z_6^2-\kappa\varepsilon z_7(\varepsilon\left\|\tilde{\Xi}\right\|-z_8)^2\\
&\quad+\kappa\varepsilon z_7z_8^2
\end{aligned}\tag{60}$$

To show that $e(t)$, $e_P(t)$, $\tilde{\Theta}(t)$, and $\tilde{\Xi}(t)$ are bounded, we require $\dot{V}\left(e,\ e_P,\ \tilde{\Theta},\ \tilde{\Xi}\right) < 0$. Thus, it follows that

$$\begin{cases} \|e\| > z_2 + \sqrt{z_2^2 + \dfrac{z_3 z_4^2 + \gamma z_5 z_6^2 + \kappa z_7 z_8^2}{z_1}} = \zeta \\ \|e_P\| > z_4 + \sqrt{z_4^2 + \dfrac{z_1 z_2^2 + \gamma z_5 z_6^2 + \kappa z_7 z_8^2}{z_3}} = \beta \\ \left\|\tilde{\Theta}\right\| > z_6 + \sqrt{z_6^2 + \dfrac{z_1 z_2^2 + z_3 z_4^2 + \kappa z_7 z_8^2}{\gamma z_5}} = \xi \\ \left\|\tilde{\Xi}\right\| > z_8 + \sqrt{z_8^2 + \dfrac{z_1 z_2^2 + z_3 z_4^2 + \gamma z_5 z_6^2}{\kappa z_7}} = \chi \end{cases} \tag{61}$$

Therefore, there exists a compact set Υ where

$$\Upsilon = \left\{\left(e,\ e_P,\ \tilde{\Theta},\ \tilde{\Xi}\right) : \|e\| \le \zeta,\ \|e_P\| \le \beta, \left\|\tilde{\Theta}\right\| \le \xi, \left\|\tilde{\Xi}\right\| \le \chi\right\} \tag{62}$$

that contains the origin $\left(e,\ e_P,\ \tilde{\Theta},\ \tilde{\Xi}\right)$.

Then $\dot{V}\left(e,\ e_P,\ \tilde{\Theta},\ \tilde{\Xi}\right) < 0$ when $\left(e,\ e_P,\ \tilde{\Theta},\ \tilde{\Xi}\right)$ is outside of Υ. Thus, any trajectory $\left(e,\ e_P,\ \tilde{\Theta},\ \tilde{\Xi}\right)$ starts from inside of Υ will remain in Υ for all the future time [35]. Therefore, Υ is an invariant set [36]. Also, any trajectory $\left(e,\ e_P,\ \tilde{\Theta},\ \tilde{\Xi}\right)$ starts from outside of Υ will approach the largest invariant set Υ as $t \to \infty$ [35]. According to the LaSalle's Invariance Principle that $e(t)$, $e_P(t)$, $\tilde{\Theta}(t)$, and $\tilde{\Xi}(t)$ are uniformly bounded. Therefore, the BOMAL in (43) is stable.

ACKNOWLEDGMENT

The authors would like to thank the anonymous reviewers for their insightful comments.

REFERENCES

[1] L. C. Jaw and J. D. Mattingly, *Aircraft Engine Controls: Design, System Analysis, and Health Monitoring*. Reston, VA, USA: AIAA, 2009.

[2] D. C. Saluru, R. K. Yedavalli, and R. K. Belapurkar, "Active fault tolerant model predictive control of a turbofan engine using C-MAPSS40k," in *Proc. Legged Locomotion; Mech. Syst.; Mechatronics, Mechatronics Aquatic Environments; MEMS Control; Model Predictive Control; Modeling Model-Based Control Adv. IC Engines*, vol. 2, Oct. 2012, pp. 349–358.

[3] M. Pan, L. Cao, W. Zhou, J. Huang, and Y.-H. Chen, "Robust decentralized control design for aircraft engines: A fractional type," *Chin. J. Aeronaut.*, vol. 32, no. 2, pp. 347–360, Feb. 2019, doi: 10.1016/j.cja.2018.08.004.

[4] X. Du, X.-M. Sun, Z.-M. Wang, and A.-N. Dai, "A scheduling scheme of linear model predictive controllers for turbofan engines," *IEEE Access*, vol. 5, pp. 24533–24541, 2017, doi: 10.1109/ACCESS.2017.2764076.

[5] H. Chen, X. Wang, H. Wang, N. Gu, M. Zhu, and S. Yang, "Inverted decoupling and LMI-based controller design for a turboprop engine with actuator dynamics," *Chin. J. Aeronaut.*, vol. 33, no. 6, pp. 1774–1787, Jun. 2020, doi: 10.1016/j.cja.2020.01.012.

[6] K. Miao, X. Wang, and M. Zhu, "Full flight envelope transient main control loop design based on LMI optimization," in *Proc. Aircr. Engine; Fans Blowers*, vol. 1, Sep. 2020, Art. no. V001T01A035.

[7] J. Liu, X. Wang, M. Zhu, and K. Miao, "Multivariable adaptive control method for turbofan engine with dynamic and input uncertainties," *J. Eng. Gas Turbines Power*, vol. 143, no. 7, Mar. 2021, Art. no. 071027, doi: 10.1115/1.4049296.

[8] B. Yang, X. Wang, and P. Sun, "Non-affine parameter dependent LPV model and LMI based adaptive control for turbofan engines," *Chin. J. Aeronaut.*, vol. 32, no. 3, pp. 585–594, Mar. 2019, doi: 10.1016/j.cja.2018.12.031.

[9] T. Sun and X.-M. Sun, "An adaptive dynamic programming scheme for nonlinear optimal control with unknown dynamics and its application to turbofan engines," *IEEE Trans. Ind. Informat.*, vol. 17, no. 1, pp. 367–376, Jan. 2021, doi: 10.1109/TII.2020.2979779.

[10] J. Kong, B. Niu, Z. Wang, P. Zhao, and W. Qi, "Adaptive output-feedback neural tracking control for uncertain switched MIMO nonlinear systems with time delays," *Int. J. Syst. Sci.*, vol. 52, p. 13, pp. 2813–2830, Apr. 2021, doi: 10.1080/00207721.2021.1909775.

[11] W. Qi, G. Zong, and W. X. Zheng, "Adaptive event-triggered SMC for stochastic switching systems with semi-Markov process and application to boost converter circuit model," *IEEE Trans. Circuits Syst. I, Reg. Papers*, vol. 68, no. 2, pp. 786–796, Feb. 2021, doi: 10.1109/TCSI.2020.3036847.

[12] W. Su, B. Niu, H. Wang, and W. Qi, "Adaptive neural network asymptotic tracking control for a class of stochastic nonlinear systems with unknown control gains and full state constraints," *Int. J. Adapt. Control Signal Process.*, vol. 35, no. 10, pp. 2007–2024, Jul. 2021, doi: 10.1002/acs.3304.

[13] W. Gai, Y. Zhou, M. Zhong, C. Sheng, and J. Zhang, "Simple adaptive control with an adaptive anti-windup compensator for the unmanned aerial vehicle attitude control," *IEEE Access*, vol. 8, pp. 52323–52332, 2020, doi: 10.1109/ACCESS.2020.2979741.

[14] M. Zhu, X. Wang, X. Pei, S. Zhang, Z. Dan, N. Gu, S. Yang, K. Miao, H. Chen, and J. Liu, "Modified robust optimal adaptive control for flight environment simulation system with heat transfer uncertainty," *Chin. J. Aeronaut.*, vol. 34, no. 2, pp. 420–431, Feb. 2021, doi: 10.1016/j.cja.2020.03.017.

[15] R. B. Anderson, J. A. Marshall, and A. L'Afflitto, "Constrained robust model reference adaptive control of a tilt-rotor quadcopter pulling an unmodeled cart," *IEEE Trans. Aerosp. Electron. Syst.*, vol. 57, no. 1, pp. 39–54, Feb. 2021, doi: 10.1109/TAES.2020.3008575.

[16] A. Calise, T. Yucelen, J. Muse, and B.-J. Yang, "A loop recovery method for adaptive control," in *Proc. AIAA Guid., Navigat., Control Conf.*, Aug. 2009, p. 5967.

[17] C. Hanson, M. Johnson, J. Schaefer, N. Nguyen, and J. Burken, "Handling qualities evaluations of low complexity model reference adaptive controllers for reduced pitch and roll damping scenarios," in *Proc. AIAA Guid., Navigat., Control Conf.*, Aug. 2011, p. 6607.

[18] N. Nguyen, K. Krishnakumar, and J. Boskovic, "An optimal control modification to model-reference adaptive control for fast adaptation," in *Proc. AIAA Guid., Navigat. Control Conf. Exhib.*, Aug. 2008, p. 7283.

[19] K. Zhang and S.-L. Ge, "Adaptive optimal control with guaranteed convergence rate for continuous-time linear systems with completely unknown dynamics," *IEEE Access*, vol. 7, pp. 11526–11532, 2019, doi: 10.1109/ACCESS.2019.2892427.

[20] H. Yi and Q. Zhang, "An optimal fuzzy control method for nonlinear time-delayed batch processes," *IEEE Access*, vol. 8, pp. 42608–42618, 2020, doi: 10.1109/ACCESS.2020.2976869.

[21] N. T. Nguyen, "Optimal control modification for robust adaptive control with large adaptive gain," *Syst. Control Lett.*, vol. 61, no. 4, pp. 485–494, Apr. 2012, doi: 10.1016/j.sysconle.2012.01.009.

[22] N. Nguyen, A. Ishihara, V. Stepanyan, and J. Boskovic, "Optimal control modification for robust adaptation of singularly perturbed systems with slow actuators," in *Proc. AIAA Guid., Navigat., Control Conf.*, Aug. 2009, p. 5615.

[23] N. T. Nguyen, "Verifiable adaptive control with analytical stability margins by optimal control modification," in *Proc. AIAA Guid., Navigat., Control Conf.*, Aug. 2010, p. 7770.

[24] N. T. Nguyen and S. N. Balakrishnan, "Bi-objective optimal control modification adaptive control for systems with input uncertainty," *IEEE/CAA J. Automatica Sinica*, vol. 1, no. 4, pp. 423–434, Oct. 2014, doi: 10.1109/JAS.2014.7004669.

[25] N. T. Nguyen, "Multi-objective optimal control modification adaptive control method for systems with input and unmatched uncertainties," in *Proc. AIAA Guid., Navigat., Control Conf.*, Jan. 2014, p. 454.

[26] P. V. Kokotovic, J. O'Reilly, and H. K. Khalil, *Singular Perturbation Methods in Control: Analysis and Design*. Orlando, FL, USA: Academic, 1986.

[27] H. Schlichting and K. Gersten, *Boundary-Layer Theory*. Berlin, Germany: Springer, 2017.

[28] N. T. Nguyen, *Model-Reference Adaptive Control: A Primer*. Cham, Switzerland: Springer, 2018.

[29] J. W. Chapman, T. M. Lavelle, R. D. May, J. S. Litt, and T. H. Guo, "Toolbox for the modeling and analysis of thermodynamic systems (T-MATS) user's guide," Glenn Res. Cent, Cleveland, OH, USA, Tech. Rep. NASA/TM-2014-216638, 2014.

[30] W. P. Visser and M. J. Broomhead, "GSP, a generic object-oriented gas turbine simulation environment," in *Proc. ASME Turbo Expo.*, Munich, Germany, 2000, Art. no. V001T01A002.
[31] M. Zhu and X. Wang, "An integral type μ synthesis method for temperature and pressure control of flight environment simulation volume," in *Proc. ASME Turbo Expo.*, Charlotte, NC, USA, 2017, Art. no. V006T05A006.
[32] M. Zhu, X. Wang, Z. Dan, S. Zhang, and X. Pei, "Two freedom linear parameter varying μ synthesis control for flight environment testbed," *Chin. J. Aeronaut.*, vol. 32, no. 5, pp. 1204–1214, 2019, doi: 10.1016/j.cja.2019.01.017.
[33] M. Zhu, X. Wang, S. Yang, H. Chen, K. Miao, and N. Gu, "Two degree-of-freedom μ synthesis control with Kalman filter for flight environment simulation volume with sensors uncertainty," in *Proc. ASME Turbo Expo.*, Phoenix, AZ, USA, 2019, Art. no. V006T05A002.
[34] M. Zhu, X. Wang, K. Miao, X. Pei, and J. Liu, "Two degree-of-freedom μ synthesis control for turbofan engine with slow actuator dynamics and uncertainties," *J. Phys., Conf. Ser.*, vol. 1828, no. 1, Feb. 2021, Art. no. 012144, doi: 10.1088/1742-6596/1828/1/012144.
[35] H. K. Khalil and J. W. Grizzle, *Nonlinear Systems*. Upper Saddle River, NJ, USA: Prentice-Hall, 2002.
[36] P. A. Ioannou and J. Sun, *Robust Adaptive Control*. Upper Saddle River, NJ, USA: Prentice-Hall, 1995.

MEIYIN ZHU was born in Sichuan, China. He received the B.S. degree from the Southwest University of Science and Technology, Mianyang, China, in 2014, and the Ph.D. degree from Beihang University, Beijing, China, in 2021.

From 2019 to 2020, he was a Visiting Scholar at the University of Waterloo, Canada. He is currently a Postdoctoral Researcher with the Beihang Hangzhou Innovation Institute Yuhang. He has authored one book, more than 26 articles (seven SCIE, 15 EI), and ten inventions. His current research interests include dynamic modeling and control design of aeroengine, dynamic modeling and control design of altitude ground test facilities, model reference adaptive control, μ synthesis control, and robust control.

XI WANG was born in Shanxi, China. He received the Ph.D. degree from Northwestern Polytechnical University, Xian, China, in 1998. He is currently a Professor with the School of Energy and Power Engineering, Beihang University, Beijing, China. He is a member of the Basic Research Group of two major aircraft projects. He is an Expert of two engines major special projects at the Third Research Institute, China Aerospace Science and Industry Corporation. Currently, his research achievements includes nine national patents for invention, 150 papers published in core journals and international conferences (12 SCI, 100 EI), and more than 80 key scientific research projects undertaken by aviation and aerospace research plants and institutes. In addition, he has undertaken a major project of two engines, a number of national major project plans and a sub-project of a major project of two engines. His current research interests include aero-engine dynamic mathematical model, control system modeling, control law design, control system fault diagnosis, and fault tolerant design.

SHUBO YANG was born in Urumqi, China. He received the Ph.D. degree in engineering from Beihang University, in 2020. He is currently a Postdoctoral Researcher with Beihang University. His current research interests include control design and dynamic system modeling and simulation.

KEQIANG MIAO was born in Jiangsu, China. He is currently pursuing the Ph.D. degree in aeroengine modeling and intelligent control design with Beihang University.

XITONG PEI was born in Hebei, China. He received the B.S. degree from the China University of Mining and Technology, Beijing, China, in 2012, and the M.S. degree from Beihang University, Beijing, in 2015, where he is currently pursuing the Ph.D. degree in aeroengine modeling and intelligent control design.

JIASHUAI LIU was born in Hebei, China. He is currently pursuing the Ph.D. degree in aeroengine modeling and intelligent control design with Beihang University.

LOUYUE ZHANG received the B.S. degree from the China University of Mining and Technology, Beijing, China, in 2019. He is currently pursuing the master's degree with the School of Energy and Power Engineering, Beihang University. His research interests include engine control, testing, condition monitoring, and fault diagnosis.